RESEARCH ARTICLE

The potential impact of carboxylic-functionalized multi-walled carbon nanotubes on trypsin: A Comprehensive spectroscopic and molecular dynamics simulation study

Maryam Noordadi[1], Faramarz Mehrnejad[1]*, Reza H. Sajedi[2], Majid Jafari[1], Bijan Ranjbar[3]

1 Department of Life Science Engineering, Faculty of New Sciences & Technologies, University of Tehran, Tehran, Iran, **2** Department of Biochemistry, Faculty of Biological sciences, Tarbiat Modares University, Tehran, Iran, **3** Department of Biophysics, Faculty of Biological sciences, Tarbiat Modares University, Tehran, Iran

* Mehrnejad@ut.ac.ir

Abstract

In this study, we report a detailed experimental, binding free energy calculation and molecular dynamics (MD) simulation investigation of the interactions of carboxylic-functionalized multi-walled carbon nanotubes (COOH-f-MWCNTs) with porcine trypsin (pTry). The enzyme exhibits decreased thermostability at 330K in the presence of COOH-f-MWCNTs. Furthermore, the activity of pTry also decreases in the presence of COOH-f-MWCNTs. The restricted diffusion of the substrate to the active site of the enzyme was observed in the experiment. The MD simulation analysis suggested that this could be because of the blocking of the S1 pocket of pTry, which plays a vital role in the substrate selectivity. The intrinsic fluorescence of pTry is quenched with increase in the COOH-f-MWCNTs concentration. Circular dichroism (CD) and UV–visible absorption spectroscopies indicate the ability of COOH-f-MWCNTs to experience conformational change in the native structure of the enzyme. The binding free energy calculations also show that electrostatics, π-cation, and π-π stacking interactions play important roles in the binding of the carboxylated CNTs with pTry. The MD simulation results demonstrated that the carboxylated CNTs adsorb to the enzyme stronger than the CNT without the–COOH groups. Our observations can provide an example of the nanoscale toxicity of COOH-f-MWCNTs for proteins, which is a critical issue for *in vivo* application of COOH-f-MWCNTs.

Introduction

Carbon-based nanomaterials have unique atomic conformation, high volume-surface ratio, high electrical conductivity, good optical features, mechanical stability, and easy functionalization capacity. Nowadays, they have attracted considerable attention in nanobiotechnological and nanomedical applications [1–6]. Carbon nanotubes (CNTs) are widely used in different fields of nano-biosensors, biomolecular recognition devices, drug and gene delivery, and

cancer therapy [7–11]. The excellent surface areas and layered and hollow structure of CNTs show that they can be ideal supporting drug molecules or gene transports via chemical or physical adsorption. Therefore, investigations of interactions of CNTs with drugs and biomolecules have increased biosafety issues for *in vivo* therapeutic applications [12–15]. However, the introduction of CNTs into biological systems can raise some questions about the potential risks of CNTs in futuristic medical and biological applications [16–20]. Despite astounding advances in industrial applications, the poor solubility of CNTs in water drastically limits effective biomedical applications. Hence, functionalization of CNTs makes them amenable for further binding of additional biomolecules, significantly increasing their biochemical and biophysical properties [21–23].

Previous studies have shown that adsorption of bio-macromolecules such as nucleic acids and proteins onto the surface of CNTs determines their cellular uptake and modulates the toxicity of CNTs [24–30]. The surface effects of CNTs on the structure and activity of proteins depend on their size, curvature, and chemistry [14, 31, 32]. To date, there are numerous studies on the interactions of CNTs with proteins [25, 27, 33, 34]. These studies have indicated that CNTs create disorders in the normal function of proteins and have some adding or reducing features, which are specific to proteins. Therefore, CNTs can affect the normal performance of proteins.

The porcine trypsin (Enzyme Commission (EC) Number 3.4.21.4) is an important serine protease enzyme. It expresses in the pancreatic cells as an inactive proenzyme (called Trypsinogen) and has 223 amino acid residues arranged in two six-stranded beta barrels [35]. The residues His-57, Asp-102, and Ser-195 were located in the active site of pTry. According to previous studies, the residues 184–195 (Loop1), 213–228 (Loop2), and 169–175 (Loop 3) form the S1 pocket in the enzyme. The pocket contains a negatively charged residue (Asp-189), which stabilizes the side chains of the positively charged residues in the substrate (Fig 1). It was concluded that the pocket plays a vital role in the substrate selectivity [36].
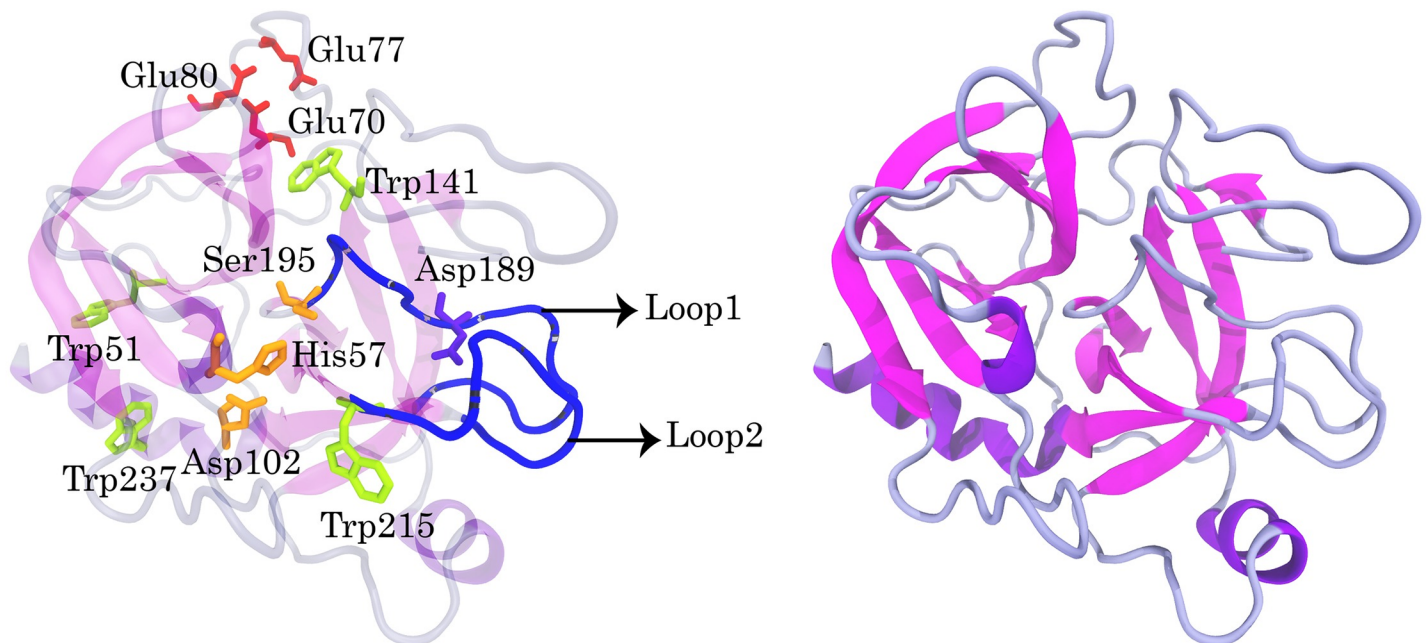

Fig 1. Left, the positions of the catalytic triad, tryptophan residues and structure of the S1 pocket of trypsin consists of residues 184–195 (Loop 1), 213–228 (Loop 2). Loop 3 (169–175) is not shown. Right, the native structure of trypsin (PDB ID: 1FNI).

The enzyme is extensively applied in different fields, including physiological processes, apoptosis, haemostasis, signal transduction, immune response, and food industry [37]. Previous studies have demonstrated that various nanoparticles can affect the enzymatic activity of pTry [38–40]. To the best of our knowledge, data has not been found about the potential impact of COOH-f-MWCNTs on the enzyme structure and activity. Considering the various uses of carbon nanotubes in medical and industrial applications, the study of the effect of COOH-f-MWCNTs on the trypsin enzyme seems to be necessary. In this work, we evaluate the mechanisms of interaction between COOH-f-MWCNTs and pTry by CD, fluorescence, UV–visible absorption spectroscopies, and MD simulations. Using a combination of experimental and theoretical techniques, we found that COOH-f-MWCNTs decrease enzyme activity in a dose-dependent manner and significantly influence the overall structure of the enzyme. The experimental and MD simulations results used in this study can provide a good perspective on the collision of trypsin with carboxylic-functionalized multi-walled carbon nanotubes.

Materials and methods

Materials

The porcine trypsin (Merck, Darmstadt, Germany) was dissolved in 20 mM Tris (2-Amino-2-(hydroxymethyl)-1, 3-propanediol, Trometamol, THAM, Tris base) buffer, pH 8.0 to form a $5.0 \times 10^{-5} \text{ M}^{-1}$ solution. The casein solution (1% (w/v)): 0/5 g of casein (Merck, Darmstadt, Germany) was suspended in 40 ml of Tris buffer and was entirely dissolved by placing on a water bath for 20 min. The solution was cooled and made up to 50 ml with Tris buffer. Trichloroacetic acid (TCA 10% (w/v)): 5 g TCA (Sigma, St. Louis, MO, USA) was dissolved in 50 ml dH_2O. COOH-f-MWCNTs (OD: 20–30 nm, Length: 10–30 μm, SSA: >110 m^2/g, Content of -COOH: 2.73 wt % were dissolved in ultrapure water (based on the TEM image of S1 Fig) using an urtra-sonicator prior to the experiment. Purity Multi-walled nanotubes>98wt %) were obtained from Iranian Nanomaterials Pioneers, Mashhad, Iran. Tris was purchased from Sigma (St. Louis, MO, USA).

Molecular dynamics simulation

The initial coordinates of pTry were obtained from the Protein Data Bank (PDB ID: 1FNI) (Fig 1) [35]. A double-walled carbon nanotube (DWCNT) (the armchair with a (9, 9) inner tube and (14, 14) outer tube) with terminal carboxylation was used. The carbon atoms were modelled as uncharged Lennard-Jones particles, and described using parameters for the atoms of aromatic carbon. Four distinct simulation systems for COOH-f-DWCNT-pTry, each consisting of a COOH-f-DWCNT and a pTry molecule were prepared. In system 1, COOH-f-DWCNT was placed at an appropriate distance from the S1 pocket (Fig 2). In system 2, COOH-f-DWCNT was positioned in the opposite direction to system 1 (Fig 2). The direction of COOH-f-DWCNT in this system was in the same orientation as the docking calculation results. In system 3 and system 4, COOH-f-DWCNT was placed in the different relative orientations (S2 Fig). To identify the effects of the–COOH functional groups on the enzyme structure, four distinct simulation systems containing the non-functionalized DWCNT ((the armchair with a (9, 9) inner tube and (14, 14) outer tube)) and pTry were also prepared (S3 Fig). The orientation of DWCNT to the enzyme in the Model 1, Model 2, Model 3 and Model 4 was the same as the system 1, system 2, system 3 and system 4, respectively. To obtain comparative results, the enzyme was simulated in pure water. All MD simulations were performed using the GROMACS simulation software, version 5.1.2 [41, 42] with the OPLS/AA force field [43]. The enzyme and the enzyme-DWCNT complexes were solved in a box (with dimensions 10nm×10nm×10nm) using the extended simple point charge (SPC/E) [44] water model. The sufficient numbers of sodium (Na+) and chloride (Cl−) ions were used to neutralize all systems. The pressure and temperature were kept
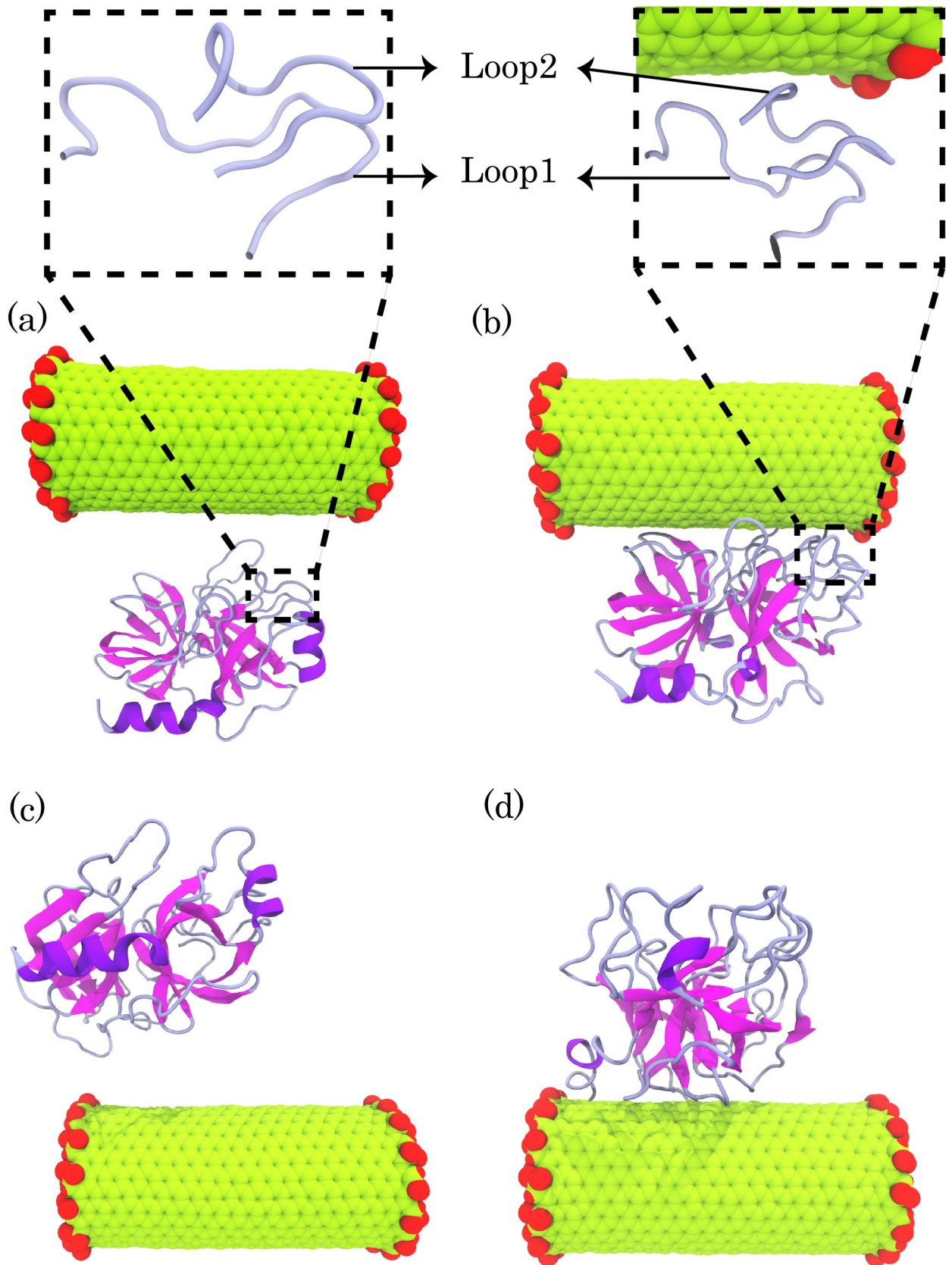
Fig 2. (a) and (b) the first and the last snapshots of trajectory in system 1, respectively. (c) and (d) the first and last snapshots of trajectory in system 2, respectively.

close to the intended values (1 bar and 300 K) using the Berendsen algorithm with $\tau_P = 0.5$ and $\tau_T = 0.1$ and ps, respectively [45]. All bonds lengths were maintained constant with the LINCS algorithm [46]. For all non-bonded interactions, a short-range spherical cut off 1 nm were used. The long-range interactions were calculated by the Particle Mesh Ewald (PME) method [47]. To energy minimization of the system, the steepest descent algorithm was applied. After minimizing the systems, the canonical (NVT) ensemble was conducted for 300 ps. All MD simulation systems were then equilibrated using an isothermal–isobaric (NPT) for 500 ps. The simulation length for each COOH-f-DWCNT-enzyme and DWCNT-enzyme system was 200 ns and 50 ns, respectively.

Binding free energy calculations

The binding free energy ($\Delta G_{binding}$) between pTry and CNTs was calculated by the molecular mechanics/Poisson- Boltzmann Surface Area (PBSA) method [48]. The binding energy was obtained using the following equation:

$$\Delta G_b = \Delta G_{complex} - (\Delta G_{pTry} + \Delta G_{CNT}) \tag{1}$$

where ΔG_b is the MM-PBSA binding energy, $\Delta G_{complex}$ is the total free energy of the CNT-pTry complexes, and ΔG_{pTry} and ΔG_{CNT} are the total free energy of pTry and CNTs, respectively. The polar binding energy ($\Delta G_{polar\ binding}$), non-polar binding energy ($\Delta G_{non-polar\ binding}$), and total binding energy ($\Delta G_{binding}$) were calculated by the following equations

$$\Delta G_{polar\ binding} = \Delta G_{electrostatic} + \Delta G_{pols} \tag{2}$$

$$\Delta G_{non-polar\ binding} = \Delta G_{van\ der\ Waals} + \Delta G_{npols} \tag{3}$$

$$\Delta G_{binding} = \Delta G_{polar\ binding} + \Delta G_{non-polar\ binding} \tag{4}$$

where ΔG_{pols} is the electrostatic part of the free energy of solvation and ΔG_{npols} is the non-electrostatic part of the free energy of solvation.

Fluorescence measurements

All fluorescence spectra were recorded on a Cary eclipse fluorescence spectrophotometer (Carry eclipse, Varian, Australia) equipped with a 10-mm quartz cell and a 150-W xenon lamp. The photo multiplier tube (PMT) voltage was medium, and the excitation and emission slit widths were set to 5.0 nm. The excitation wavelength was adjusted to 280 nm and the emission wavelength scans ranged from 290 to 600 nm. The scan speed was 600 nm.min^{-1}. Intrinsic fluorescence was recorded using 2.0×10^{-5} M^{-1} of pTry in 20 mM Tris, pH 8.0, in the absence and presence of different concentrations of COOH-f-MWCNTs. In fluorescence measurements, all spectra containing the COOH-f-MWCNTs-pTry solutions were subtracted with the COOH-f-MWCNTs solution spectra and were smoothed.

In this regard, the binding parameters determined with the Stern–Volmer plot by using Eq 5:

$$\frac{F_o - F}{F} = k_q \times \tau_o[Q] = 1 + K_{sv}[Q] \tag{5}$$

where F_o and F define the steady-state fluorescence intensities in the absence and presence of a quencher, respectively. k_q is the quenching rate constant of the enzyme, and τ_0 (10^{-8} s) is the average life time of the enzyme without any quencher, [Q] is the concentration of the quencher, K_{SV} is the Stern–Volmer quenching constant, [49] and other form of the Stern-Volmer equation is 6: [50]

$$Log\left[\frac{F_o - F}{F}\right] = Log\,K_A + n\,Log[Q] \tag{6}$$

and thermodynamic Eq 7:

$$\Delta G^0 = -RT\,K_A \tag{7}$$

K_A is the binding constant, and n is binding sites of the COOH-f-MWCNTs-pTry complex, ΔG^0 is the free energy change, R is the gas constant (8.314 Jmol^{-1}k^{-1}), and T is the absolute temperature.

UV–visible absorption measurements

All UV-visible absorption spectra were recorded on a Nanodrop 2000 spectrophotometer (Thermo Scientific™ Nanodrop™) equipped with a 10-mm quartz cell. The UV–visible spectra of pTry in the absence and presence of COOH-f-MWCNTs were recorded in the range of 190–420 nm at 298 K. The enzyme concentration was 2.0×10^{-5} M^{-1} for the experiment. In the UV–visible absorption measurements, all spectra containing the COOH-f-MWCNTs-pTry solutions were subtracted with the COOH-f-MWCNTs solution spectra and were smoothed.

Far-UV circular dichroism measurements

The CD spectra were operated over the range of wavelength of 190–250 nm with a J-810 CD spectropolarimeter (Jasco, Tokyo, Japan) using a quartz cell with a path length of 1 mm. The scanning speed was set to 200 nm.min^{-1}. The results were reported as molar ellipticity [θ] (degree cm^2.dmol^{-1}), based on the average amino acid residue weight (MRW) of pTry and the data were smoothed using the Jasco J-810 software, which includes a fast Fourier-transform noise reduction routine. The secondary structure contents of the enzyme in percentage were estimated by using the software provided by the JASCO software version 1.10.02. In CD spectroscopy studies, all spectra containing the COOH-f-MWCNTs-pTry solutions were subtracted with the COOH-f-MWCNTs solution spectra and were smoothed.

Protease activity assay

The activity of pTry was measured at pH 8.0 in 20 mM Tris buffer at room temperature. The enzymatic reaction was evaluated with 100 μg.ml^{-1} pTry concentration and 1% casein as substrate in the final volume of 500 μl. After 10 minutes incubation, the enzymatic reaction was stopped by addition of 500 μl of 10% TCA and then the supernatant absorbance was determined in 280 nm [51]. The activity of protease can be determined as the quantity micromoles of tyrosine released from substrate by the enzyme in per minute under the assigned assay conditions [52].

Enzyme kinetics

The Michaelis–Menten kinetics of native pTry and apparent kinetics of the enzyme in the present of COOH-f-MWCNTs were determined. A solution of casein in 20 mM Tris buffer (pH 8.0) was serially diluted to establish a substrate range from 0 to 15 mg.ml^{-1}. The enzyme

was added to individual tubes containing the casein solutions in the absence or presence of COOH-f-MWCNTs. The reaction was allowed to proceed for 10 minutes at room temperature. The absorbance was measured at 280 nm and the acceleration of product alteration was designated with the use of the primitive rate of the reactions. By using the Michaelis–Menten equation (GraphPad, prism 6, USA) and plotting reaction rate (V) against concentration of the substrate, the parameters (K_m and V_{max}) were obtained. The k_{cat} was calculated by using the following equation:

$$V\max/[E] \tag{8}$$

where [E] define as the initial enzyme concentration. (The molar mass of pTry was considered 23,300 g.mol^{-1}).

Unalterable thermo-inactivation of pTry

The inconvertible heat inactivation of the enzyme was accomplished by placing of the pTry samples at the temperature 313 K in the absence and presence of COOH-f-MWCNTs. For thermal stability evaluation, variant concentrations of COOH-f-MWCNTs were examined on the thermostability of the enzyme. At regular intervals, the samples were removed and cooled on ice for 30 minutes and the residual activity was then determined at 298 K under the assay conditions. In each experiment, the residual activity of the enzyme that incubated at 40°C for 0 min considered as control (with 100% activity). The k_{in} and the half-life the enzyme inactivation were determined as follows:

$$\text{Ln}(Activity) = \text{Ln}(Activity)_0 - \text{K}_{in}t \tag{9}$$

and

$$\text{Half} - \text{life} = 0.693/\text{K}_{in} \tag{10}$$

Statistical analysis

All experiments were performed in triplicate and data are shown as mean ± SD. Statistical analysis was performed according to the Student's t -test and one-way ANOVA analysis followed by the Dunnett's multiple comparison tests. The probability values of $P < 0.05$ were considered as significance.

Results and discussion

First, steady state fluorescence was performed to obtain data on the tertiary structural properties of pTry. The porcine trypsin is a globular protein that contains four tryptophan (TRP) residues (51, 141, 215, and 237), which are used as intrinsic fluorophores (Fig 1) [53]. To examine the conformational properties of pTry in the aqueous COOH-f-MWCNT solution, the enzyme molecules were allowed to interact with various concentrations of COOH-f-MWCNT, and the emergent fluorescence emission maxima were measured (Fig 3). In our investigations, the fluorescence emission of pTry was obtained at 339 nm, upon excitation at 280 nm. Available data indicate that the fluorescence intensity of the enzyme decreases upon addition of various concentrations of COOH-f-MWCNTs, while the fluorescence emission spectra of the enzyme exhibit a slight blue shift upon addition of COOH-f-MWCNTs (Fig 3(A)). COOH-f-MWCNTs had not significant emission in fluorescence measurements (Fig 3(B)). It is clear that the fluorescence of pTry was obviously quenched after the addition of COOH-f-MWCNTs (Fig 3(C)). To obtain this quenching mechanism, the results were computed with the Stern–Volmer equation (inset upper right in Fig 3(A)). The plot, at various concentrations of COOH-f-MWCNTs was
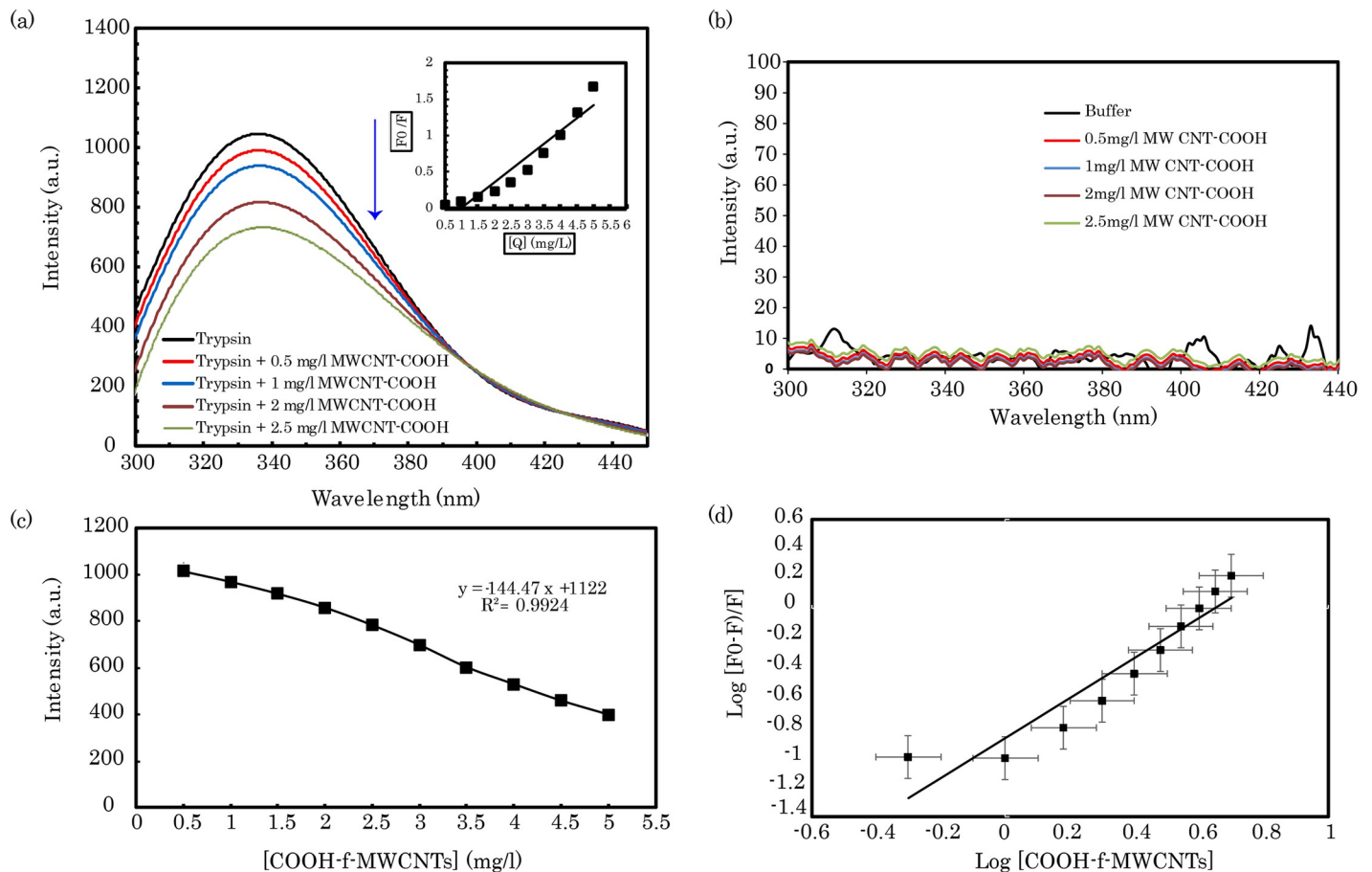
Fig 3. (a) Fluorescence spectra of the COOH-f-MWCNTs-pTry system. Conditions: λ_{ex} = 280 nm, pH 8.0; $C_{trypsin}$ 2.0×10^{-5} M, C_{CNTs} are in the total volume of the reaction mixture; pH 8.0, T = 298 K. (b) Emission spectra of COOH-f-MWCNTs systems alone. (c) The plot of fluorescence quenching for trypsin with the concentration of COOH-f-MWCNTs. (d) The logarithmic plot of trypsin with the concentration of COOH-f-MWCNTs. Data are shown as mean values ± S.D.

linear, which suggests that the type of quenching of pTry follows single mechanism kinetics. As shown in Fig 3(C), the k_{SV} and k_q ($k_{q\,=\,}k_{SV}/\tau_0$) values of the COOH-f-MWCNTs-pTry complex were obtained as 0.352 ($\times 10^8$ M^{-1}) and 0.352 ($\times 10^{16}$ M^{-1}.s^{-1}), respectively. In this study, the order of magnitude of k_q was 0.352×10^{16}. However, the maximum scatter collision quenching constant, k_q, of various quenchers with the biopolymer was 2×10^{10} (M^{-1}.s^{-1}) [54]. Therefore, static quenching drove the fluorescence quenching process, which is associated with the formation of the ground state complex between the enzyme and COOH-f-MWCNTs, in compatibility with the UV-visible absorptions. Eq 9 was used to obtain the binding parameters. Fig 3(D) shows the plots of log [(F_0-F)/F] versus log [COOH-f-MWCNTs]. The values of slope and intercept were 1.3 and –0.871, respectively. Since the molecular weight of COOH-f-MWCNTs was not definite in the COOH-f-MWCNTs-pTry samples, we used λ as a pseudo molar concentration pursuant to previous studies [50]. According to the size of COOH-f-MWCNTs in this work (OD: 20–30 nm; length: 10–30 μm), the value of λ was no more than 1×10^{-8}. The value of intercept was -0.871, which revealed that K_A is equal to 0.135/λ. The numerical value of n indicates that there is a significant binding site for COOH-f-MWCNTs on pTry. On the other hand, the value of K_A (1.35×10^7 M^{-1}) shows that there are strong interactions between COOH-f-MWCNTs and enzyme: these are significantly stronger than the interactions between HO-MWCNTs and bovine serum albumin (BSA) (1.39×10^4 M^{-1}) in the same studies [55]. The

value of ΔG^0 in the formation of the COOH-f-MWCNTs-pTry complex was −40 kJ.mol^{-1}. This value indicates a spontaneous exothermic reaction, as expected. The fluorescence quenching of the enzyme demonstrates that the tryptophan residues in the hydrophobic core were gradually exposed to the aqueous medium with increase in the concentration of COOH-f-MWCNTs. In addition, the small blue shift in the position of the fluorescence emission spectra indicates that the COOH-f-MWCNTs-pTry interactions might occur around the tryptophan residues, which were found to be located in a more hydrophobic microenvironment after the addition of COOH-f-MWCNTs [56–58].

To study the effects of COOH-f-MWCNTs on the pTry structure, UV-visible absorption was used. The aromatic amino acid residues of pTry contribute to UV absorbance at approximately 274 nm with respect to their π-π* transition [59]. Therefore, the UV absorption peak around 278 nm suggests the buried aromatic amino acid residues of the enzyme (Fig 4(A)). The UV-visible spectra indicate that increase in the concentration of COOH-f-MWCNTs in
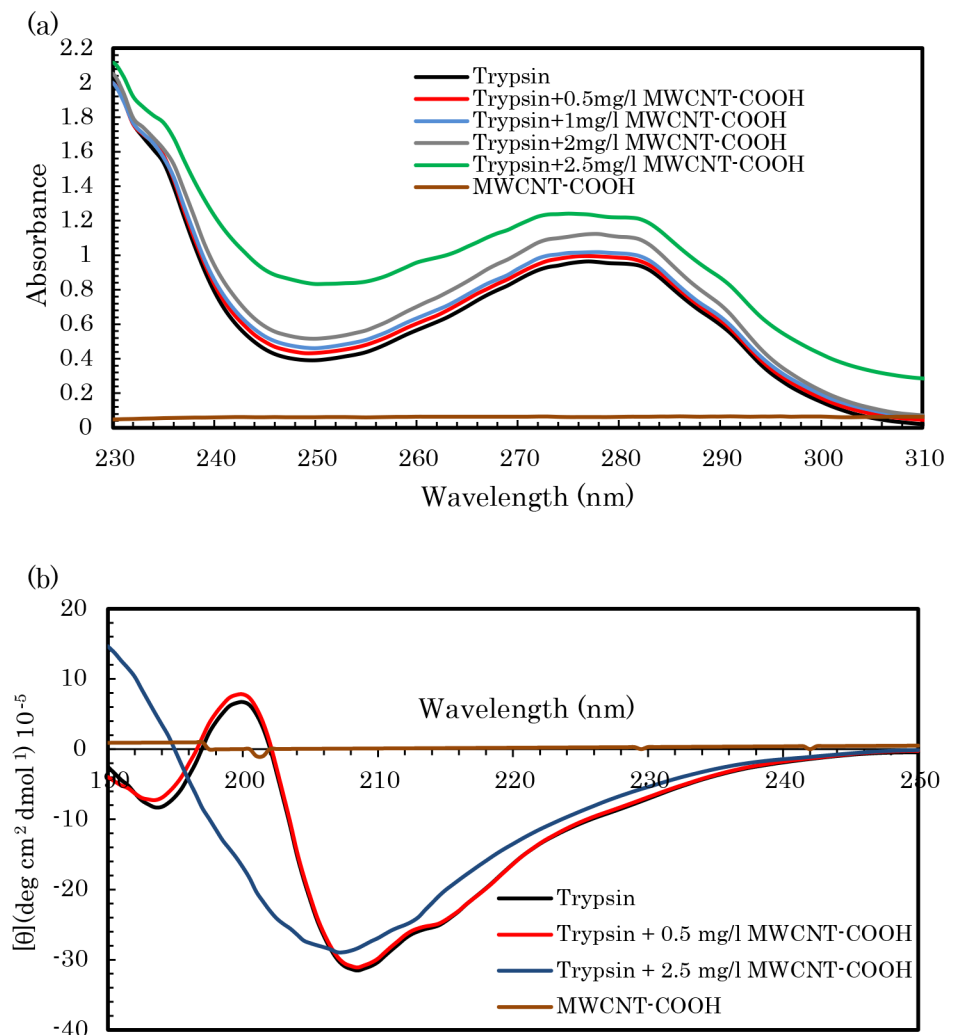
Fig 4. (a) UV–visible absorption spectra of trypsin. $C_{trypsin}$ = 2.0 × 10^{-5} M, C_{CNTs} are in the total volume of the reaction mixture; pH 8.0, T = 298 K. (b) CD spectra of trypsin and COOH-f-MWCNTs-pTry mixtures. $C_{trypsin}$ = 1 × 10^{-4} M. C_{CNTs} are in the total volume of the reaction mixture; pH 8.0, T = 298 K. Data are shown as mean values ± S.D.

https://doi.org/10.1371/journal.pone.0198519.g004

the pTry solution significantly increase the intensity of the UV absorption spectra. It suggests that COOH-f-MWCNTs and pTry form a complex, as the pTry molecules get adsorbed on the surface of COOH-f-MWCNTs: this indicates that the side chains of residues were partly changed [3, 60]. These results confirm that the static quenching mechanism is in high agreement with the fluorescence findings.

CD is an important tool for rapid monitoring of the folding and unfolding states and secondary structures of proteins in solutions [61–63]. The far-UV CD spectra of proteins (185 −250 nm wavelengths) were used to provide data about the composition of the secondary structure components [63]. To obtain further information about the effects of COOH-f-MWCNTs on the secondary structural contents of pTry, the CD spectra (far-UV) were used for two COOH-f-MWCNTs-pTry mixtures (0.5 and 2.5 mg. L^{-1}). From CD spectra analysis, it is clear that the alpha-helix structures decreased upon increase in the COOH-f-MWCNTs concentration (Fig 4(B)). Table 1 indicates that COOH-f-MWCNTs could induce the secondary structure changes in pTry by the distribution of hydrogen bonding networks.

The relative activity of the enzyme was determined in the presence of different concentrations of COOH-f-MWCNTs (0–2 mg. L^{-1}) (Fig 5(A)). As can be observed, the relative activity of pTry was approximately 92%, 79%, and 74%, in the presence of 0.5 mg/l, 1 mg/l, and 2 mg/l of COOH-f-MWCNTs, respectively.

The enzyme showed a Michaelis-Menten type of kinetics when hydrolyzed with casein in the absence and presence of COOH-f-MWCNTs. As shown in Table 2, the kinetic parameters do not undergo significant variations after addition of COOH-f-MWCNTs: only a slight increase and decrease in K_m and k_{cat} of pTry is observable. This results in slight decrease in k_{cat}/K_m, in the COOH-f-MWCNT aqueous solution as compared to the free form. The results of the enzyme kinetics show that increase in the K_m value may be due to diffusion limitations and steric hindrance of the active site. Decrease in k_{cat} could be due to the restricted diffusion of the substrate to the active site and/or the higher structural rigidity of the enzyme due to the presence of the nanotube [64].

The effect of COOH-f-MWCNTs on the thermal stability of pTry has also been studied. In the presence of two concentrations of COOH-f-MWCNTs, the pTry enzyme exhibits decrease in thermostability at 330 K compared with the free form (Fig 5(B)). The plots of the Ln of residual activity versus time are linear. Therefore, a first-order decay process under these conditions was observed. The half-life of the enzyme was 9.65 min in the free form, while in the presence of 1 and 2 mg. L^{-1} of COOH-f-MWCNTs it was 8.68 min and 7.98 min, respectively (Table 3).

To provide information about the enzyme adsorption on the COOH-f-DWCNT surface, we calculated the center of mass (COM) distance between the enzyme and COOH-f-DWCNT during MD simulations (Fig 6(A)). As demonstrated, during the early steps of the simulations the distances between COOH-f-DWCNT and the enzyme decreased drastically in all the systems, indicating the early adsorption of the enzyme on the surface of COOH-f-DWCNT. We also computed the C_{alpha} root-mean-square-deviation (RMSD) of the enzyme for determining the stability of the enzyme over the simulations (Fig 6(B)). As can be seen in system 2, the

Table 1. The influence of COOH-f-MWCNTs on the secondary structure of trypsin.

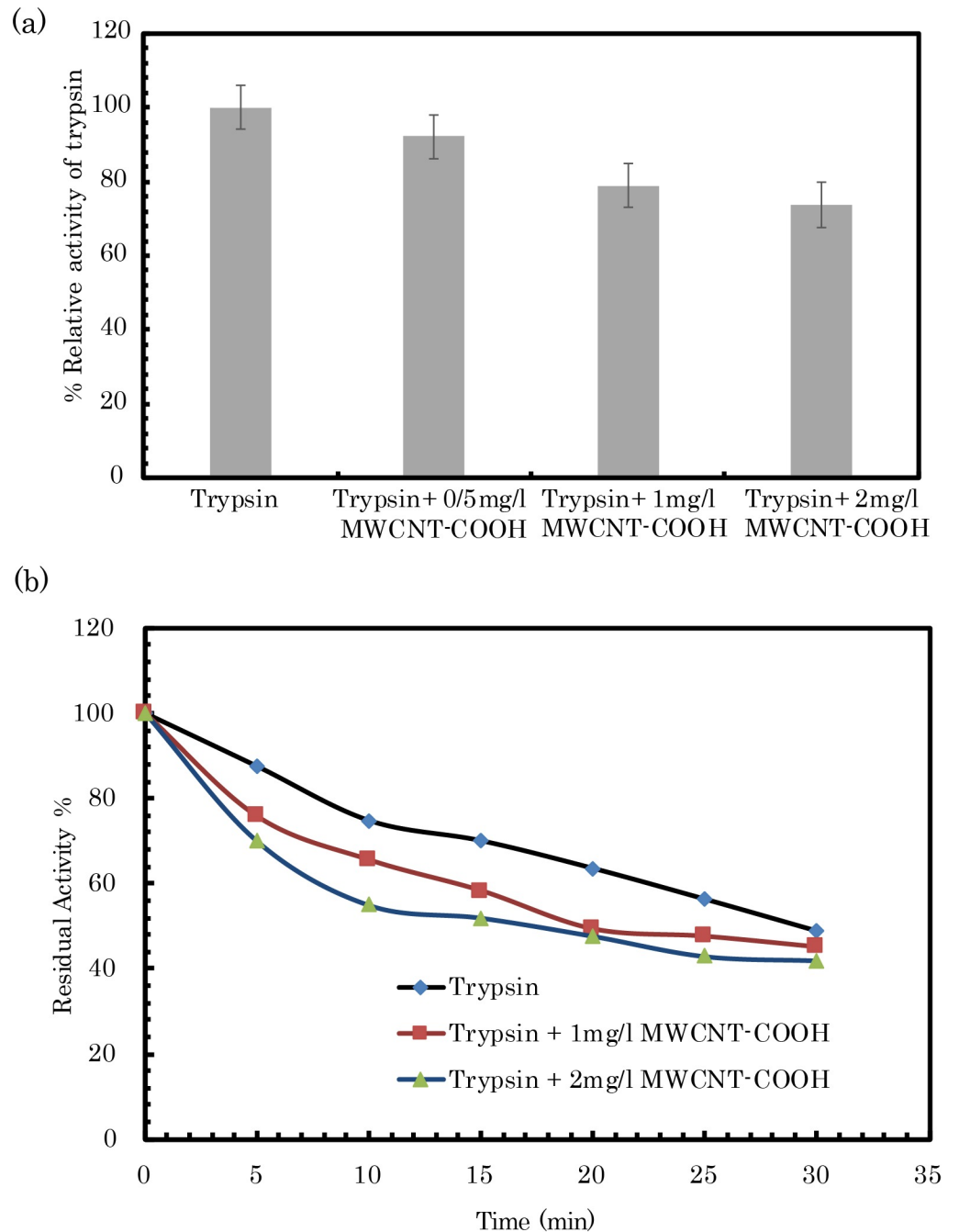| System (experimental)	α-Helix (%)	β-Sheet (%)	Random coil (%)	Others
Trypsin	16.2	34.7	28.0	21.1
Trypsin+0.5 mg.L^{-1} CNT	16.0	35.6	28.9	19.5
Trypsin+2.5 mg.L^{-1}CNT	5.2	59.9	34.9	-

Fig 5. (a) Effects of COOH-f-MWCNTs on the activity of trypsin. (b) The thermostability of trypsin in the presence of COOH-f-MWCNTs. pH 8.0, T = 330 K: C_{trypsin} (control) = 100 μg/ml. C_{CNTs} are in the total volume of the reaction mixture; pH 8.0, T = 298 K. Data are shown as mean values ± S.D.

RMSD values of pTry increased in the presence of COOH-f-DWCNT, which indicates rapid divergence from the starting structure. This observation demonstrated that the fluctuations of pTry were more in system 2 than in other systems (Fig 6(B)). In system 1, there was no significant difference between the RMSD values of the system and the enzyme in water. However, the RMSD values for the enzyme in systems 3 and 4 were approximately the same as each

Table 2. Effect of COOH-f-MWCNTs on the kinetic parameters of the porcine trypsin. The values were calculated using GraphPad Prism.

System	K_m (mg.ml^{-1})	k_{cat} (min^{-1})	k_{cat}/K_m)	R square
Trypsin	3.9	37.79	9.7	0.988
Trypsin+2.5 mg.L^{-1} CNT	4.24	33.72	8.0	0.993

other and the enzyme was more stable than the other systems during the simulation time. Based on the RMSD results, it can be suggested that the results of the MD simulations depend on the starting position of COOH-f-DWCNT.

By calculating Define Secondary Structure of Proteins (DSSP) [65] from the MD simulation, we found that there was a notable decrease in the alpha-helix contents of pTry upon interaction with COOH-f-DWCNT. This was in agreement with our experimental results (Fig 7) and with previous studies [66, 67]. To further validate the DSSP findings, we also obtained the residue secondary structure of the enzyme in each system using the STRIDE web server [68]. Zhao et al. reported that the carboxylated CNTs increase the beta-sheet structures and decrease the alpha-helical contents of alpha-chymotrypsin [69]. According to the data obtained from DSSP and the STRIDE server, over the MD simulation time, the α-helices of the enzyme were unstable and adopted the 3_{10}-helix, coil, and turn structures (Fig 7 and S4 Fig). Because of the docking method could anticipate the preferred direction of the carbon nanotube to the enzyme and since the importance of the S1 pocket of the enzyme, we focused on systems 1 and 2. The MD simulation analyses for the other orientations and systems were provided in the supplementary information. As demonstrated in Fig 7, Tyr-234 and Trp-237, which are located in the alpha-helix structure of the enzyme, lost the helicity and the beta-sheet structure containing Trp-215 was changed to turn. Therefore, the quenching and slight blue shift observed for pTry—discussed earlier- could be due to the interactions, which increase the local concentrations of COOH-f-MWCNTs around the tyrosine and tryptophan residues of pTry. Meanwhile, in all four COOH-f-DWCNT systems, pTry lost its 3_{10}-helix structure consisting of residues 56 to 58 ("AHC"), where His-57 in the active site of the enzyme adopted a turn structure. The specificity of pTry is usually determined by the residues Asp-189 (Loop 1), Gly-216, and Gly-226 (Loop2) [36]. As indicated in Fig 7, Gly-216 and Gly-226 (in system 1) with structure of turn and beta-sheet respectively adopted the coil structure. These data suggest that COOH-f-DWCNT induced a significant change in the overall conformation of pTry. In systems 1 and 3, although COOH-f-DWCNT had the different starting orientation to the enzyme, the S1 pocket was blocked by COOH-f-DWCNT (Fig 2 and S2 Fig). In general, COOH-f-DWCNT, independent from its initial orientation, was adsorbed to the two directions of the enzyme (the docking results orientation and the opposite direction), indicating that the mentioned two directions of the enzyme are the adsorption sites for COOH-f-DWCNT. In system 1, Loop 3 did not show significant interactions with COOH-f-DWCNT: therefore, we focused on the structural changes in the Loop 1 and Loop 2 of the S1 pocket, whereas in system 3, Loop 2 and Loop 3 remarkably interact with COOH-f-DWCNT (S2 Fig).

Table 3. Inactivation rate constant (k_{in}) and half-life of the trypsin in the absence and presence of COOH-f-MWCNTs at T = 330 K.

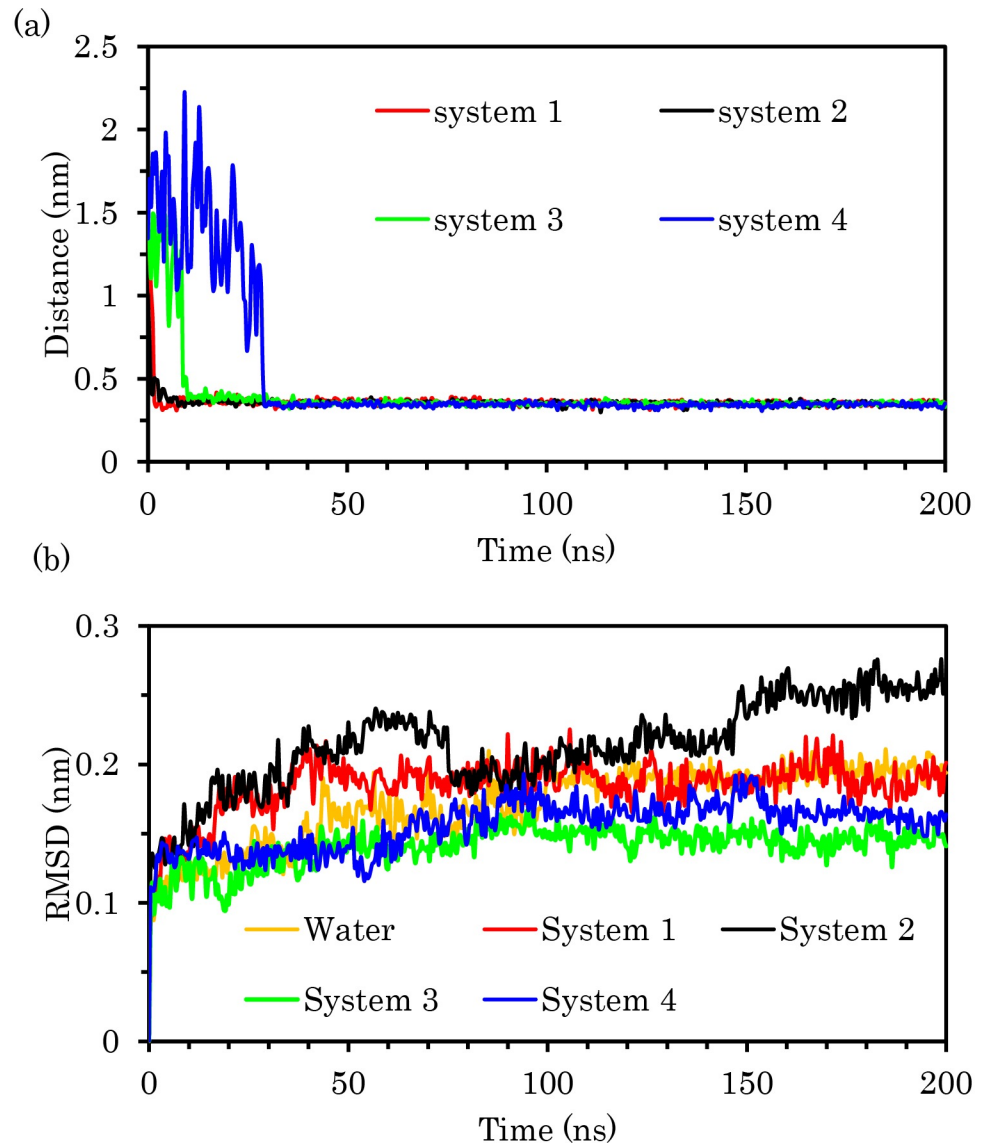| System	k_{in} (min^{-1})	Half-life (min)	R square
Trypsin	0.0718	9.65	0.973
Trypsin+1 mg.L^{-1} CNT	0.0798	8.68	0.979
Trypsin+2mg.L^{-1} CNT	0.0868	7.98	0.954

(a)

(b)

Fig 6. (a) Center of mass (COM) distances between the enzyme and COOH-f-DWCNT as a function of time (b) The RMSD of C-α of trypsin during the simulation time.

We first calculated distance between the center of mass (COM) of COOH-f-DWCNT and the Loops in system 1 (Fig 8(A)). As can be seen in Fig 8(A), the distance of Loop 1 and Loop 2 from COOH-f-DWCNT decreases rapidly after 10 ns: compared to Loop1, Loop 2 is closer to the surface of COOH-f-DWCNT because the cationic residues in Loop 2 could interact with the COOH groups of COOH-f-DWCNT. We also calculated the number of hydrogen bonds between the S1 pocket and COOH-f-DWCNT in system 1 and system 3 over the simulation time (Fig 8(B) and S5 Fig). The results in Fig 8(B) show that the negatively charged carboxyl groups of COOH-f-DWCNT can form hydrogen bonds with the polar residues of the S1 pocket, such as the Gln-221, Lys-222, and Lys-224 residues.

The contribution energy per residue of the S1 pocket to the total binding free energies is listed in Table 4. These results confirm the role of residues of the S1 pocket in the absorption process. Eight residues of the S1 pocket were in contact with COOH-f-DWCNT, while most of them were
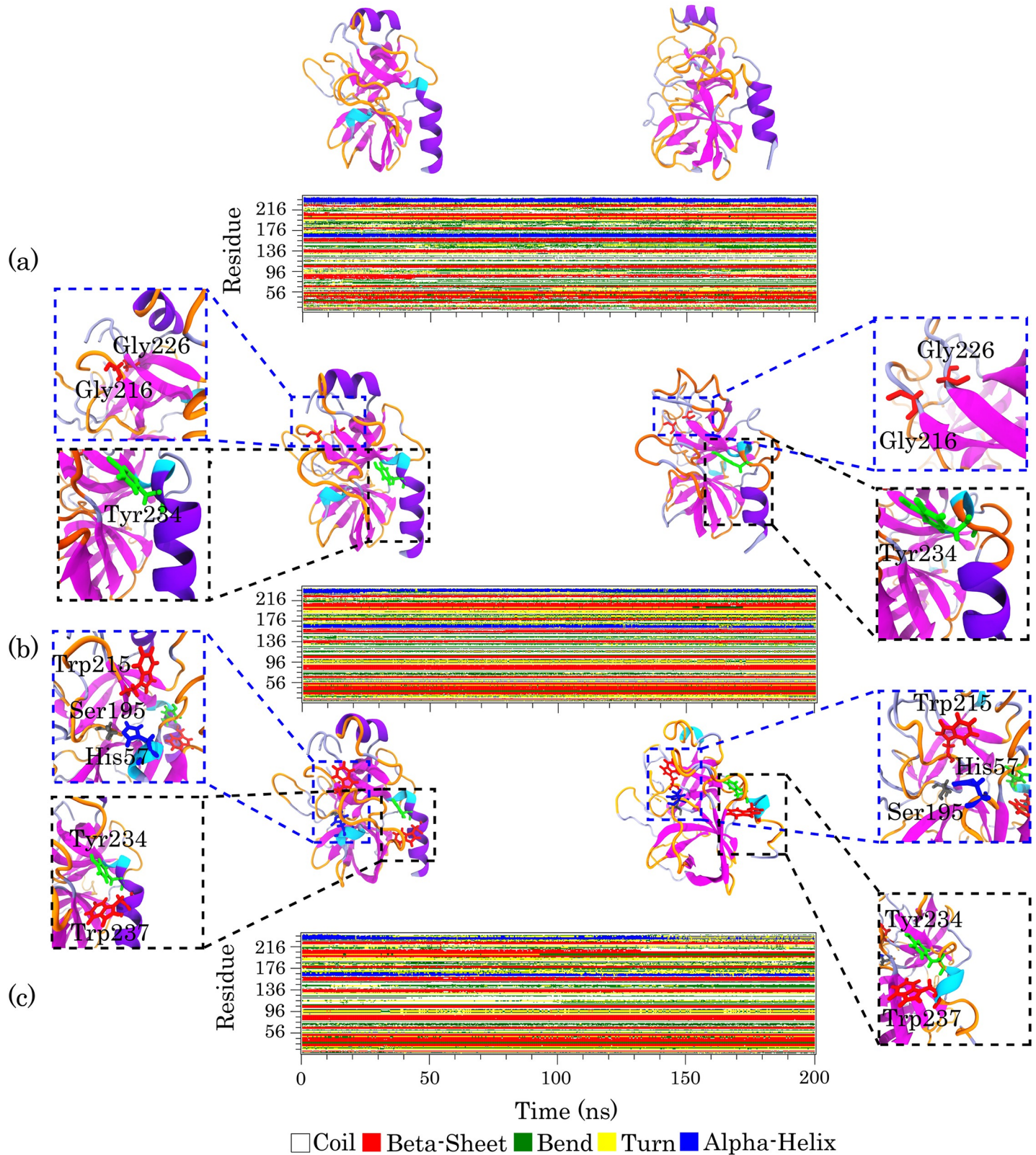
Fig 7. Time evolution of the secondary structure of the enzyme during MD simulations generated by DSSP for (a) the enzyme in water (as control), (b) system 1, and (c) system 2. The cartoon model of the first and the last snapshots of MD of the enzyme structure are shown in left and right respectively. Changes of secondary structure of several residues are shown, for instance. The alpha helix, 3_{10} helix, beta sheet, turns, and coil structures are colored in violet, cyan, magenta, orange, and ice blue, respectively. For the DSSP analysis of the enzyme in system 3 and system 4, refer to the supplementary information.

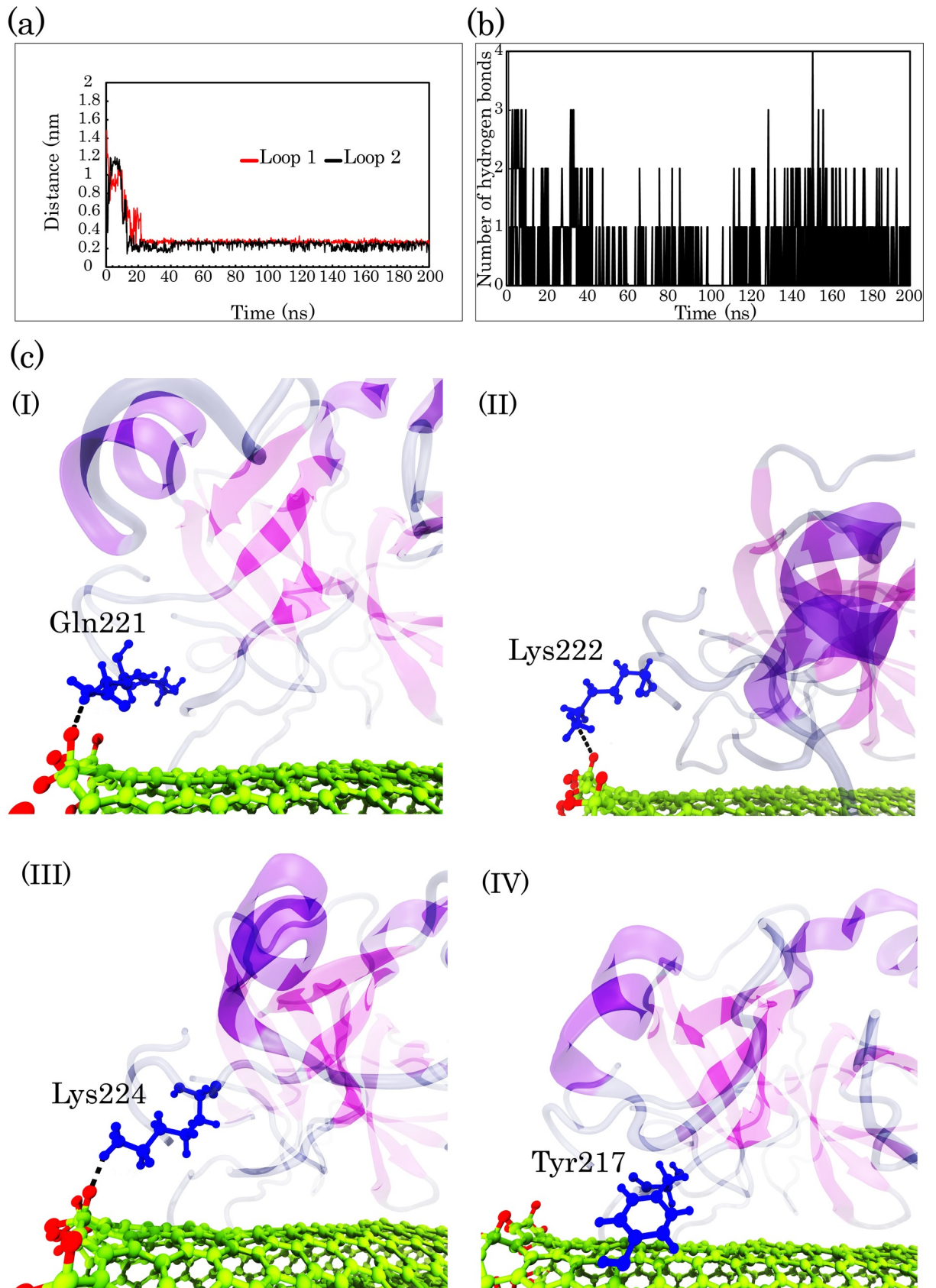**Fig 8. MD simulations indicate interaction between COOH-f-DWCNT and S1 pocket of the enzyme.** (a) Minimum distance between Loop 1 and Loop 2 of S1 pocket with COOH-f-DWCNT in system 1 over the simulation time (for analysis of minimum distance between Loops with COOH-f-DWCNT in system 3, refer to the supplementary information). (b) The number of hydrogen bonds between S1 pocket and COOH groups of COOH-f-DWCNT in system 1 as function of time. (c) Local snapshots from hydrogen binding interaction by (I) Gln-221, (II) Lys-222, and (III) Lys-224 and π-π stacking interaction by (IV) Tyr-217.

basic and polar residues. The Lys-188, Lys-222, and Lys-224 residues with $\Delta G_{binding} < -90$ kJ.mol^{-1} and Tyr-217 and Gln-221 with $\Delta G_{binding} < -8.0$ kJ.mol^{-1} had more effective contributions to the total binding energy. In addition, the contribution energy of each S1 pocket residue in system 3 has been shown in the supplementary information (S1 Table).

The aromatic residue Tyr-217, which is located at Loop 2 of the S1 pocket, can interact with the aromatic rings on the surface of COOH-f-DWCNT by π-π stacking interactions (Fig 8 (C)). We were able to demonstrate the representative snapshots of π-π stacking attractions and hydrogen bonds, which contributed to the interaction process between COOH-f-DWCNT and the S1 pocket (Fig 8(C)). These interactions can change the structure of the S1 pocket in consistence with the DSSP findings, and correspondingly influence performance of the active site. Similarly, a recent study has also shown that the interactions between the COOH groups of COOH-SWCNT and several specific basic and polar residues of the cytochrome P450 enzyme (CYP3A4) can inhibit its catalytic activity. The authors believe this suggests electrostatic interactions have an important role during the binding process [70].

Consequently, the results highlight that the S1 pocket adsorbs on the COOH-f-DWCNT surface through electrostatic interactions, and hydrogen bonds and Loop 2 plays a crucial role in the adsorption of the enzyme on the nanotube surface. As a result, a combination of different interaction types contributes to the blocking of the S1 pocket by COOH-f-DWCNT. Fig 2 shows representative snapshots of the first (a and c) and the last (b and d) steps of the trajectory in system 1. The figure supports the important role of Loop 2 in the adsorption process of the S1 pocket on the carbon nanotube. It is clear that conformational changes in the S1 pocket can influence substrate accessibility correspondingly. Overall, our results confirm that COOH-f-DWCNT adsorbs onto the S1 pocket with a strong tendency: it can be the reason for decrease in the activity of pTry in the presence of COOH-f-DWCNT (See S2 Fig for system 3).

Previous studies have shown that the π-cation interactions—the interactions between aromatic rings on the surface of carbon nanotube and the cationic group of basic residues—and π-π-stacking interactions—a non-covalent attractive force between two aromatic rings—contribute to the binding of CNT to proteins [70, 71]. As demonstrated in Fig 9, the guanidinium group of Arg-117, Arg-125 (in system 2), and Arg-62 (in system 1) and the amine group of Lys-60 (in system 1) and Lys-159 (in system 2) can participate in the multiple interactions—such as π-cation interactions and hydrogen bonds—with COOH-f-DWCNT (Fig 9). Additionally, the aromatic residues Tyr-151 and Tyr-217 (system 1) and Tyr-29 (system 2) can interact with the aromatic rings of COOH-f-DWCNT by the π-π-stacking interactions (Fig 9 panels (a) and (b)).

We computed the total binding energy, van der Waals, electrostatic and non-polar binding energies between COOH-f-DWCNT and the enzyme for all the MD simulations systems (Fig

Table 4. The binding energy ($\Delta G_{binding}$) of S1 pocket residues (kJ.mol^{-1}) in system1.

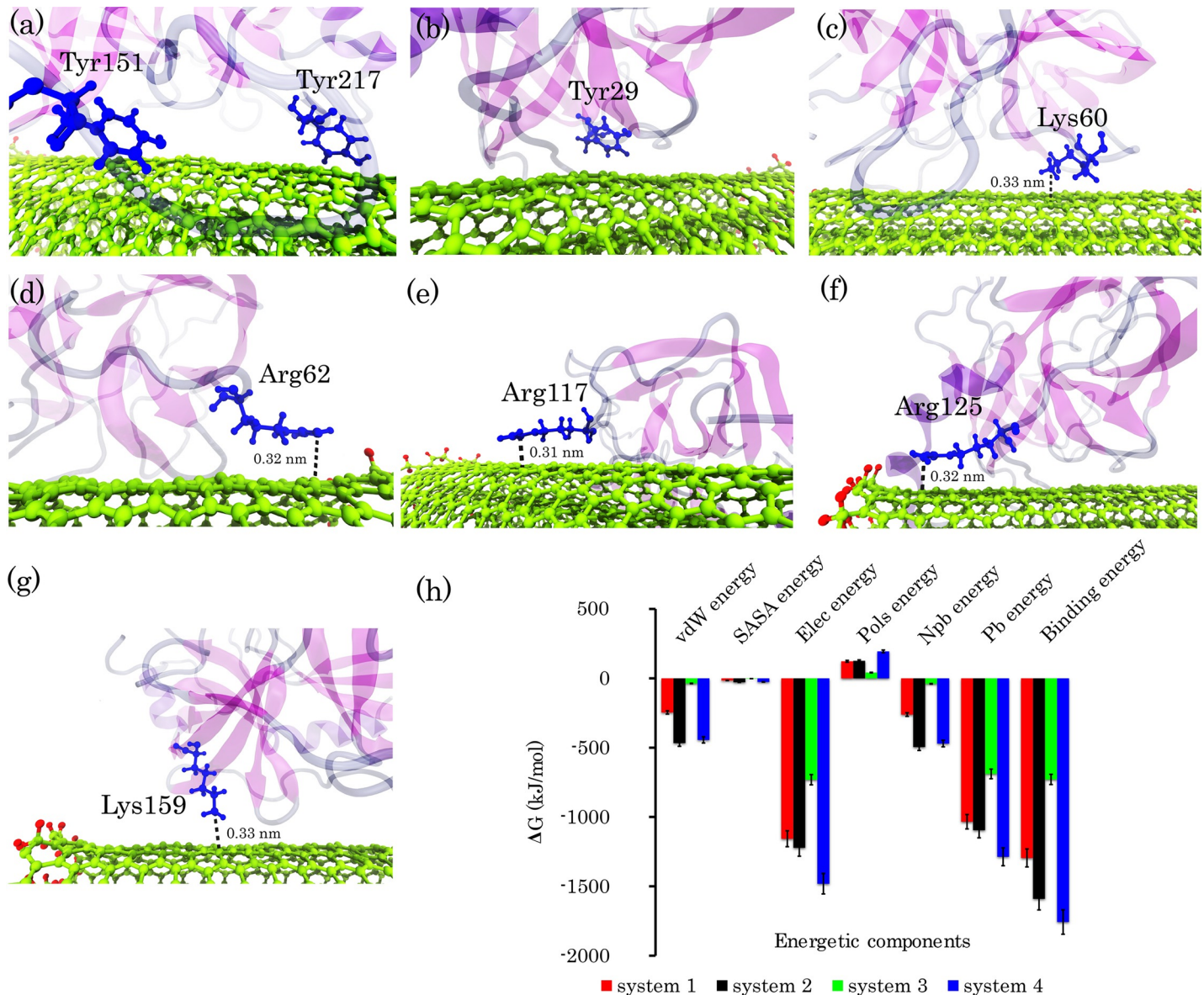| Residue	$\Delta G_{binding}$	Residue	$\Delta G_{binding}$	Residue	$\Delta G_{binding}$
Lys-188	-92.3899	Gly-219	-3.8869	Lys-222	-110.388
Gln-192	-6.4745	Cys-220	-5.3121	Lys-224	-110.823
Tyr-217	-8.4082	Gln-221	-8.8456	-	-

Fig 9. The snapshot of MD simulation outcomes shows the preferred binding sites on enzyme for COOH-f-DWCNT. π-π stacking interactions (a) Tyr 151 and Tyr 217 (system 1) (b) Tyr 29 (system 2). π–cation stacking interactions (c, d) Lys 60 and Arg 62 (system 1) (e, f, g) Arg 117, Arg 125 and Lys 159 (sysytem2). (h) Energetic components of COOH-f-DWCNT-pTry complex. vdW is van der Waals energy, SASA is non-polar energy, Elec is electrostatic energy, Pols is polar solvation energy, Npb is non-polar binding energy and Pb is polar binding energy.

9(H)). The results indicate that COOH-f-DWCNT strongly binds to the enzyme and that electrostatic interactions play important roles in interactions of the nanotube with the enzyme: this is in good agreement with previous studies [72–75]. The results also indicate that $\Delta G_{polar\ binding}$ (−1034.07 kJ.mol-1) in system 1, $\Delta G_{polar\ binding}$ (−1095.29 kJ.mol-1) in system 2, $\Delta G_{polar\ binding}$ (-689.68 kJ.mol^{-1}) in system 3, and $\Delta G_{polar\ binding}$ (-1287.11 kJ.mol^{-1}) in system 4 are favorable for the formation of the COOH-f-DWCNT-pTry complexes (Fig 9(H)), which are related to the COOH groups on COOH-f-DWCNT [76]. It may be worthwhile to point out that a combination of different interaction types contributes to the interaction process between COOH-f-DWCNT and pTry.

To gain more insight into the adsorption of pTry on the nanotube surface, we calculated the number of contacts between pTry and COOH-f-DWCNT (S5 Fig). As indicated, the number of contacts increased quickly in all the systems: this increasing trend in system 2 is more apparent during 200 ns simulation time. When the distance between one of the non-hydrogen atom residues and the CNT surface is less than 0.5 nm, the residues are identified as "contacted" and they can act as binding sites [71]. Therefore, we also computed the minimum distance and the total binding energy between each residue of the enzyme and the nanotube (Fig 10). It can be observed that a large number of residues have a distance < 0.5 nm with favorable $\Delta G_{binding}$ < -2 kJ.mol^{-1}.

Recent MD simulations have shown that the guanidinium group of the arginine residues can intercede in protein-CNT interactions [72, 73, 77]. Eugen et al. stated that Arg-112 is the most important residue in the binding of lysozyme to the surface of CNT [72]. It has been shown that the interaction sites between human myeloperoxidase and COOH-CNT contain the arginine and tyrosine residues [78]. In excellent agreement with these studies, the minimum distance analysis and the energy calculations revealed that the positively charged residues, with a minimum distance of < 0.5 nm, could make major contributors to the binding free energy (Fig 10 and S2 Table). Our results also demonstrated that the polar residues of the enzyme, such as Ser-37, Ser-39, Asn-143, Ser-147, Ser-149, Gln-192, and Gln-221 in system 1 (Fig 10 (e)) and Asn-25, Ser-26, Asn-48, Ser-122, Asn-202, Gln-204, and Gln-239 in system 2 (Fig 10(F)), can interact with the carboxyl groups of COOH-f-DWCNT. The polar residue for system 3 was Gln-175 and the related polar residues for system 4 were Asn-25, Ser-26, Thr-113, Asn-115, Ser-116, Thr-120, Thr-134, and Asn-202. Collectively, the results in Fig 10 comply with previous studies and show that these aforementioned interactions play important roles in the COOH-f-DWCNT-pTry interactions.

To identify the effects of the carboxyl groups of CNT on the enzyme structure, we also modelled four systems containing the CNT without the–COOH functional groups and the enzyme. The initial CNT orientations to the enzyme were precisely the same as they were in the COOH-f-DWCNT-pTry systems (S3 Fig). We first compared the van der Waals interactions, the electrostatic interactions and the polar and nonpolar binding energies between the carbon nanotube and the enzyme in both COOH-f-DWCNT-pTry and DWCNT-pTry systems (S3 Table). The results indicate that electrostatic interactions and polar binding energies for the COOH-f-DWCNT-pTry systems were favourable, whereas the aforementioned interactions for the systems with CNT without the–COOH groups were equal to zero. Therefore, it can be suggested that the carboxyl groups of CNT could interact with the enzyme using the electrostatic and polar interactions. In other words, COOH-f-DWCNT had more interactions with the enzyme than DWCNT. Therefore, it can be concluded that COOH-f-DWCNT could affect the enzyme structure more than the CNT without the–COOH groups. Additionally, COOH-f-DWCNT had the ability to make hydrogen bonds with the enzyme, while the CNTs without the functional groups had not this capability (Fig 8(B) and S5 Fig). In summary, the results of the hydrogen bonds and the energies indicate that COOH-f-DWCNT adsorbs to the enzyme stronger than DWCNT.

Conclusions

The interactions of COOH-f-MWCNTs with pTry were investigated in this paper by using experimental and MD simulation techniques. The results indicate that the inherent fluorescence intensity of pTry decreases in the presence of increased COOH-f-MWCNTs concentrations based on the static quenching mechanism. This is related to the formation of a COOH-f-MWCNTs-pTry complex. The CD results show that the alpha-helix structure content
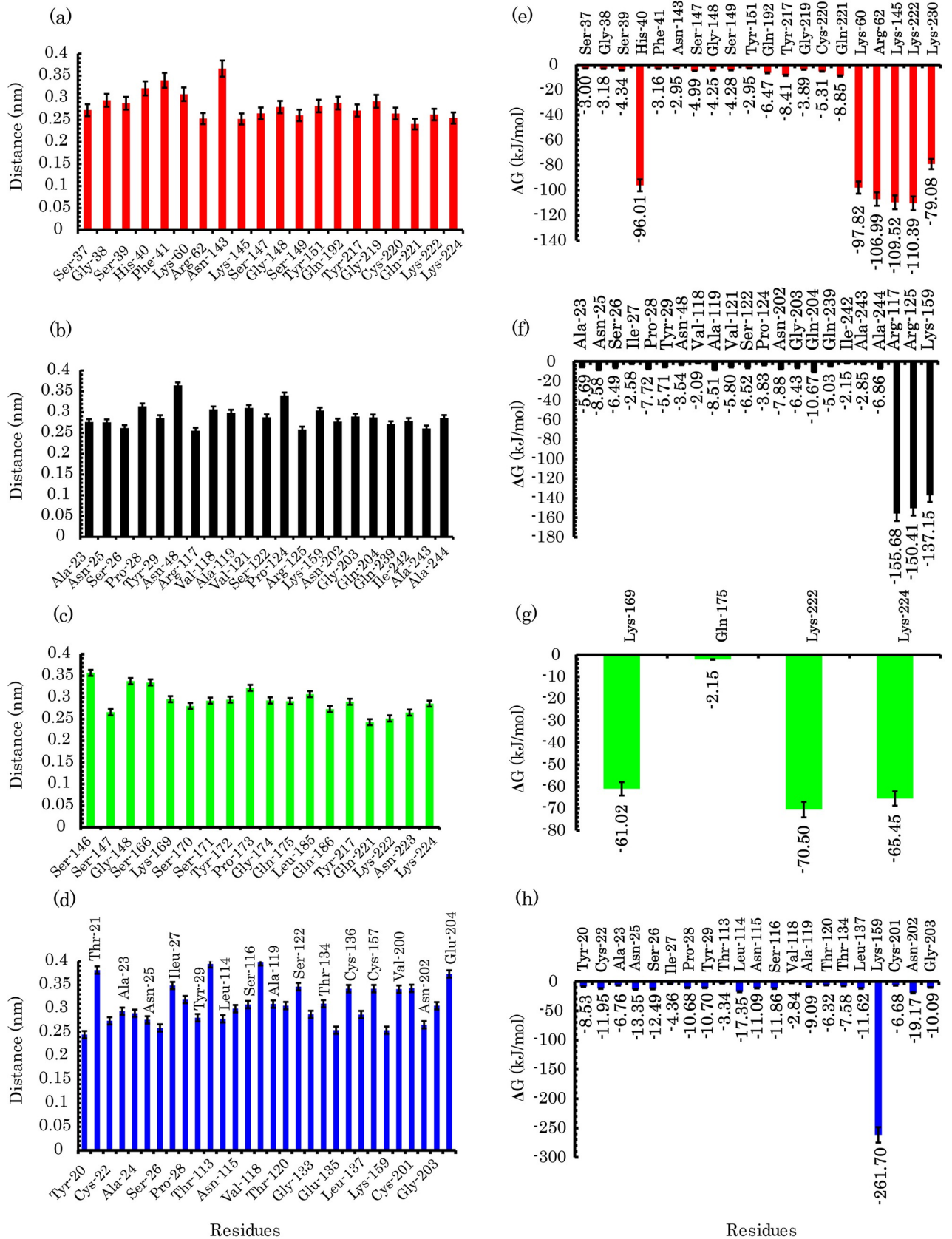
Fig 10. Adsorption process of the enzyme on the surface of COOH-f-DWCNT. (a) to (d) The minimum distance between residues and COOH-f-DWCNT in system 1, system 2, system 3 and system 4, respectively. (e) to (h) the energy residues with value of binding energy < -2 kJ.mol^{-1} in system 1, system 2, system 3 and system 4, respectively.

decreases in the presence of COOH-f-MWCNTs. Therefore, COOH-f-MWCNTs interact with the main chain of pTry and disturb the enzyme hydrogen bond networks. To ensure our experimental results, MD simulations and binding free energy calculations were done. The simulation analyses demonstrate that COOH-f-DWCNT binds to the S1 pocket of pTry and can block the active site of the enzyme. The MD simulations reveal that COOH-f-DWCNT increases the flexibility of pTry and the enzyme conformation. The binding free energy calculations demonstrate that the basic residues play an important role in the interaction of the enzyme with COOH-f-DWCNT. In summary, our experimental and MD simulations results indicate that the conformation, dynamics, activity, and stability of the enzyme are affected by COOH-f-MWCNTs. In addition, the electrostatic, π-cation, and π-π stacking interactions are the main driving forces for the enzyme binding to the surface of COOH-f-MWCNTs. Consistent with the studies above, our results demonstrated that COOH-f-DWCNT has stronger affinity to the enzyme than CNT without the–COOH groups. For toxicity investigations, this research will provide an example of nanoscale toxicity resulting from direct interference with bio-macromolecules.

Supporting information

S1 Fig. TEM image of Multi-walled nanotubes (MWNTs)–COOH functionalized (20–30 nm, Purity $>$98%, -COOH). Carboxylation of MWCNTs is one of the widely used methods to improve the solubility in aqueous solution. COOH-f-MWCNTs were dispersed in ultrapure water for characterization study and in order to reduce agglomeration. COOH-f-MWCNTs Samples was sonicated several times intermittently (30s every 2 min) using a sonicator probe (Misonix-700 Q, USA) at 30˚C. Ultraviolet- visible (UV–vis) spectra of COOH-f-MWCNTs were monitored using a Nanodrop 2000 spectrophotometer (Thermo Scientific™ Nanodrop™) equipped with a 10-mm quartz cell over the range 190–800 nm and the intensity and position of wavelength maximum was determined. COOH-f-MWCNTs did not absorb in UV-Vis region. In addition, the CNTs dispersions were analyzed using TEM to reveal the size of the individual CNTs. S1 Fig shows TEM image of COOH-f-MWCNTs dispersed in ultrapure water. It is evident, from the image that all the COOH-f-MWCNTs provide hollow and tubular shapes. Based on the TEM image of S1 Fig, it can be concluded that the COOH-f-MWCNTs dispersed in ultrapure water present diameter of about 20–30 nm.
(TIF)

S2 Fig. Two different initial configurations of COOH-f-DWCNT used in the system 3 and system 4. (a) and (b) Depict the first and last snapshots of system 3, respectively. (c) and (d) represent the first and last snapshots of the system 4, respectively. (e) The COM distance between COOH-f-DWCNT and Loop1, Loop2, and Loop3 of the S1 pocket during the MD simulations. As can be seen, Loop1 is further from COOH-f-DWCNT than Loop2 and 3.
(TIF)

S3 Fig. Snapshots of the models containing CNTs without carboxyl groups. (a), (c), (e), and (g) are the first snapshots in the Model 1, Model 2, Model 3, and Model 4, respectively. (b), (d), (f), and (h) are the last snapshots in the Model 1, Model 2, Model 3, and Model 4, respectively.
(TIF)

S4 Fig. The DSSP analysis for (a) the system 3 and (b) the system 4.
(TIF)

S5 Fig. (a) The number of hydrogen bonds between S1 pocket and -COOH groups of COOH-f-DWCNT in system 3 over the simulation time. (b) The number of contacts between COOH-f-DWCNT and the enzyme for all four systems during the MD simulation time.
(TIF)

S1 Table. The binding energy ($\Delta G_{binding}$) of residues of S1 pocket with favorable $\Delta G_{binding}$ < -2 kJ.mol^{-1} in system 3.
(PDF)

S2 Table. The contribution energy of each basic residue to the total binding energy. The residues had absolute value of binding energy < -60 kJ.mol^{-1}.
(PDF)

S3 Table. The calculated energies for the systems containing CNT with (S1, S2, S3, and S4) and without (M1, M2, M3, and M4) the carboxyl groups.
(PDF)

Acknowledgments

Author Contributions

Conceptualization: Maryam Noordadi, Faramarz Mehrnejad, Majid Jafari, Bijan Ranjbar.

Data curation: Faramarz Mehrnejad, Majid Jafari.

Formal analysis: Maryam Noordadi, Faramarz Mehrnejad, Majid Jafari.

Funding acquisition: Faramarz Mehrnejad.

Investigation: Maryam Noordadi, Faramarz Mehrnejad, Reza H. Sajedi, Bijan Ranjbar.

Methodology: Maryam Noordadi, Reza H. Sajedi, Majid Jafari.

Project administration: Faramarz Mehrnejad, Reza H. Sajedi, Bijan Ranjbar.

Supervision: Faramarz Mehrnejad.

Validation: Faramarz Mehrnejad, Reza H. Sajedi.

Writing – original draft: Maryam Noordadi, Majid Jafari.

Writing – review & editing: Faramarz Mehrnejad, Reza H. Sajedi, Bijan Ranjbar.

References

1. Mu Q, Broughton DL, Yan B. Endosomal leakage and nuclear translocation of multiwalled carbon nano-tubes: developing a model for cell uptake. Nano letters. 2009; 9(12):4370–5. https://doi.org/10.1021/nl902647x PMID: 19902917

2. Klaine SJ, Alvarez PJ, Batley GE, Fernandes TF, Handy RD, Lyon DY, et al. Nanomaterials in the environment: behavior, fate, bioavailability, and effects. Environmental toxicology and chemistry. 2008; 27 (9):1825–51. PMID: 19086204

3. Li L, Lin R, He H, Jiang L, Gao M. Interaction of carboxylated single-walled carbon nanotubes with bovine serum albumin. Spectrochimica Acta Part A: Molecular and Biomolecular Spectroscopy. 2013; 105:45–51.

4. Tonelli FM, Goulart VA, Gomes KN, Ladeira MS, Santos AK, Lorençon E, et al. Graphene-based nano-materials: biological and medical applications and toxicity. Nanomedicine. 2015; 10(15):2423–50. https://doi.org/10.2217/nnm.15.65 PMID: 26244905

5. Rutherglen C, Jain D, Burke P. Nanotube electronics for radiofrequency applications. Nat Nano. 2009; 4(12):811–9.

6. Iijima S, Ichihashi T. Single-shell carbon nanotubes of 1-nm diameter. nature. 1993; 363(6430):603.

7. Nepal D, Geckeler KE. Proteins and carbon nanotubes: close encounter in water. Small. 2007; 3 (7):1259–65. Epub 2007/05/12. https://doi.org/10.1002/smll.200600511 PMID: 17492743.

8. Zhao X, Lu D, Hao F, Liu R. Exploring the diameter and surface dependent conformational changes in carbon nanotube-protein corona and the related cytotoxicity. J Hazard Mater. 2015; 292:98–107. Epub 2015/03/24. https://doi.org/10.1016/j.jhazmat.2015.03.023 S0304-3894(15)00211-3 [pii]. PMID: 25797928.

9. Wilson NR, Macpherson JV. Carbon nanotube tips for atomic force microscopy. Nat Nano. 2009; 4 (8):483–91.

10. Liu Y, Wang H. Nanomedicine: Nanotechnology tackles tumours. Nat Nano. 2007; 2(1):20–1.

11. De La Zerda A, Zavaleta C, Keren S, Vaithilingam S, Bodapati S, Liu Z, et al. Carbon nanotubes as photoacoustic molecular imaging agents in living mice. Nature nanotechnology. 2008; 3(9):557. https://doi.org/10.1038/nnano.2008.231 PMID: 18772918

12. Wang S, Humphreys ES, Chung S-Y, Delduco DF, Lustig SR, Wang H, et al. Peptides with selective affinity for carbon nanotubes. Nat Mater. 2003; 2(3):196–200. https://doi.org/10.1038/nmat833 PMID: 12612679

13. Baker SE, Cai W, Lasseter TL, Weidkamp KP, Hamers RJ. Covalently Bonded Adducts of Deoxyribo-nucleic Acid (DNA) Oligonucleotides with Single-Wall Carbon Nanotubes: Synthesis and Hybridization. Nano Letters. 2002; 2(12):1413–7. https://doi.org/10.1021/nl025729f

14. Sekar G, Mukherjee A, Chandrasekaran N. Comprehensive spectroscopic studies on the interaction of biomolecules with surfactant detached multi-walled carbon nanotubes. Colloids Surf B Biointerfaces. 2015; 128:315–21. Epub 2015/02/25. https://doi.org/10.1016/j.colsurfb.2015.02.006 S0927-7765(15)00082-X [pii]. PMID: 25707749.

15. Bonab MI, Sardroodi JJ, Ebrahimzadeh AR, Mehrnejad F. Molecular Interactions in the Systems Com-posed of Curcumin, Water and Single-Walled Carbon Nanotube: A Molecular Dynamics Simulation Study. Journal of Computational and Theoretical Nanoscience. 2015; 12(9):2077–83.

16. Bianco A, Kostarelos K, Partidos CD, Prato M. Biomedical applications of functionalised carbon nano-tubes. Chemical Communications. 2005;(5):571–7. https://doi.org/10.1039/b410943k PMID: 15672140

17. Wenrong Y, Pall T, Gooding JJ, Simon PR, Filip B. Carbon nanotubes for biological and biomedical applications. Nanotechnology. 2007; 18(41):412001.

18. Pantarotto D, Singh R, McCarthy D, Erhardt M, Briand JP, Prato M, et al. Functionalized carbon nano-tubes for plasmid DNA gene delivery. Angew Chem Int Ed Engl. 2004; 43(39):5242–6. Epub 2004/09/30. https://doi.org/10.1002/anie.200460437 PMID: 15455428.

19. Khadem-Maaref M, Mehrnejad F, Zonoz NA, Ghahremanpour MM. Role of Hydrophobic Forces and Backbone Hydrogen Bonding on Helical Stability of Peptide Encapsulated Into Single Wall Carbon Nanotubes. Journal of Computational and Theoretical Nanoscience. 2012; 9(6):783–8.

20. Shvedova AA, Pietroiusti A, Fadeel B, Kagan VE. Mechanisms of carbon nanotube-induced toxicity: focus on oxidative stress. Toxicology and applied pharmacology. 2012; 261(2):121–33. https://doi.org/10.1016/j.taap.2012.03.023 PMID: 22513272

21. Chen RJ, Bangsaruntip S, Drouvalakis KA, Kam NW, Shim M, Li Y, et al. Noncovalent functionalization of carbon nanotubes for highly specific electronic biosensors. Proc Natl Acad Sci U S A. 2003; 100 (9):4984–9. Epub 2003/04/17. https://doi.org/10.1073/pnas.0837064100 0837064100 [pii]. PMID: 12697899; PubMed Central PMCID: PMC154284.

22. Prato M, Kostarelos K, Bianco A. Functionalized Carbon Nanotubes in Drug Design and Discovery. Accounts of Chemical Research. 2008; 41(1):60–8. https://doi.org/10.1021/ar700089b PMID: 17867649

23. Bussy C, Hadad C, Prato M, Bianco A, Kostarelos K. Intracellular degradation of chemically functiona-lized carbon nanotubes using a long-term primary microglial culture model. Nanoscale. 2016; 8(1):590–601. https://doi.org/10.1039/c5nr06625e PMID: 26647092

24. Gao H, Kong Y, Cui D, Ozkan CS. Spontaneous Insertion of DNA Oligonucleotides into Carbon Nano-tubes. Nano Letters. 2003; 3(4):471–3. https://doi.org/10.1021/nl025967a

25. Chen RJ, Zhang Y, Wang D, Dai H. Noncovalent Sidewall Functionalization of Single-Walled Carbon Nanotubes for Protein Immobilization. Journal of the American Chemical Society. 2001; 123(16):3838–9. https://doi.org/10.1021/ja010172b PMID: 11457124

26. Shannahan JH, Brown JM, Chen R, Ke PC, Lai X, Mitra S, et al. Comparison of Nanotube–Protein Corona Composition in Cell Culture Media. Small. 2013; 9(12):2171–81. https://doi.org/10.1002/smll.201202243 PMID: 23322550

27. Marchesan S, Prato M. Under the lens: carbon nanotube and protein interaction at the nanoscale. Chemical Communications. 2015; 51(21):4347–59. https://doi.org/10.1039/c4cc09173f PMID: 25621901

28. Xu Z, Zhang S, Weber JK, Luan B, Zhou R, Li J. Sequential protein unfolding through a carbon nanotube pore. Nanoscale. 2016. https://doi.org/10.1039/c6nr00410e PMID: 26899409

29. Fadel TR, Li N, Shah S, Look M, Pfefferle LD, Haller GL, et al. Adsorption of Multimeric T Cell Antigens on Carbon Nanotubes: Effect on Protein Structure and Antigen-Specific T Cell Stimulation. Small. 2013; 9(5):666–72. https://doi.org/10.1002/smll.201201684 PMID: 23090793

30. Costa PM, Fadeel B. Emerging systems biology approaches in nanotoxicology: Towards a mechanism-based understanding of nanomaterial hazard and risk. Toxicology and applied pharmacology. 2016; 299:101–11. https://doi.org/10.1016/j.taap.2015.12.014 PMID: 26721310

31. Deng ZJ, Liang M, Monteiro M, Toth I, Minchin RF. Nanoparticle-induced unfolding of fibrinogen promotes Mac-1 receptor activation and inflammation. Nat Nano. 2011; 6(1):39–44. http://www.nature.com/nnano/journal/v6/n1/abs/nnano.2010.250.html#supplementary-information.

32. Roach P, Farrar D, Perry CC. Surface Tailoring for Controlled Protein Adsorption: Effect of Topography at the Nanometer Scale and Chemistry. Journal of the American Chemical Society. 2006; 128 (12):3939–45. https://doi.org/10.1021/ja056278e PMID: 16551101

33. Salvador-Morales C, Flahaut E, Sim E, Sloan J, H. Green ML, Sim RB. Complement activation and protein adsorption by carbon nanotubes. Molecular Immunology. 2006; 43(3):193–201. https://doi.org/10.1016/j.molimm.2005.02.006 PMID: 16199256

34. Saptarshi SR, Duschl A, Lopata AL. Interaction of nanoparticles with proteins: relation to bio-reactivity of the nanoparticle. J Nanobiotechnology. 2013; 11:26. Epub 2013/07/23. https://doi.org/10.1186/1477-3155-11-26 1477-3155-11-26 [pii]. PMID: 23870291; PubMed Central PMCID: PMC3720198.

35. Deepthi S, Johnson A, Pattabhi V. Structures of porcine β-trypsin–detergent complexes: the stabilization of proteins through hydrophilic binding of polydocanol. Acta Crystallographica Section D: Biological Crystallography. 2001; 57(11):1506–12.

36. Perona JJ, Craik CS. Evolutionary divergence of substrate specificity within the chymotrypsin-like serine protease fold. Journal of Biological Chemistry. 1997; 272(48):29987–90. PMID: 9374470

37. Gombos L, Kardos J, Patthy A, Medveczky P, Szilágyi L, Málnási-Csizmadia A, et al. Probing conformational plasticity of the activation domain of trypsin: the role of glycine hinges. Biochemistry. 2008; 47 (6):1675–84. https://doi.org/10.1021/bi701454e PMID: 18193894

38. Wang S, Bao H, Yang P, Chen G. Immobilization of trypsin in polyaniline-coated nano-Fe3O4/carbon nanotube composite for protein digestion. Analytica chimica acta. 2008; 612(2):182–9. https://doi.org/10.1016/j.aca.2008.02.035 PMID: 18358864

39. Hinterwirth H, Lindner W, Lämmerhofer M. Bioconjugation of trypsin onto gold nanoparticles: effect of surface chemistry on bioactivity. Analytica chimica acta. 2012; 733:90–7. https://doi.org/10.1016/j.aca.2012.04.036 PMID: 22704381

40. Wang W-R, Zhu R-R, Xiao R, Liu H, Wang S-L. The Electrostatic Interactions Between Nano-TiO2 and Trypsin Inhibit the Enzyme Activity and Change the Secondary Structure of Trypsin. Biological Trace Element Research. 2010; 142(3):435–46. https://doi.org/10.1007/s12011-010-8823-x PMID: 20809270

41. Berendsen HJ, van der Spoel D, van Drunen R. GROMACS: a message-passing parallel molecular dynamics implementation. Computer Physics Communications. 1995; 91(1–3):43–56.

42. Abraham MJ, Murtola T, Schulz R, Páll S, Smith JC, Hess B, et al. GROMACS: High performance molecular simulations through multi-level parallelism from laptops to supercomputers. SoftwareX. 2015; 1:19–25.

43. Jorgensen WL, Maxwell DS, Tirado-Rives J. Development and testing of the OPLS all-atom force field on conformational energetics and properties of organic liquids. Journal of the American Chemical Society. 1996; 118(45):11225–36.

44. Berendsen HJC, Grigera JR, Straatsma TP. The missing term in effective pair potentials. The Journal of Physical Chemistry. 1987; 91(24):6269–71. https://doi.org/10.1021/j100308a038

45. Berendsen HJC, van der Spoel D, van Drunen R. GROMACS: A message-passing parallel molecular dynamics implementation. Computer Physics Communications. 1995; 91(1–3):43–56. http://dx.doi.org/10.1016/0010-4655(95)00042-E.

46. Hess B, Bekker H, Berendsen HJ, Fraaije JG. LINCS: a linear constraint solver for molecular simulations. Journal of computational chemistry. 1997; 18(12):1463–72.

47. Darden T, York D, Pedersen L. Particle mesh Ewald: An N· log (N) method for Ewald sums in large systems. The Journal of chemical physics. 1993; 98(12):10089–92.

48. Kumari R, Kumar R, Consortium OSDD, Lynn A. g_mmpbsa A GROMACS tool for high-throughput MM-PBSA calculations. Journal of chemical information and modeling. 2014; 54(7):1951–62. https://doi.org/10.1021/ci500020m PMID: 24850022

49. Gentili PL, Ortica F, Favaro G. Static and Dynamic Interaction of a Naturally Occurring Photochromic Molecule with Bovine Serum Albumin Studied by UV−Visible Absorption and Fluorescence Spectroscopy. The Journal of Physical Chemistry B. 2008; 112(51):16793–801. https://doi.org/10.1021/jp805922g PMID: 19367911

50. Lou K, Zhu Z, Zhang H, Wang Y, Wang X, Cao J. Comprehensive studies on the nature of interaction between carboxylated multi-walled carbon nanotubes and bovine serum albumin. Chemico-biological interactions. 2016; 243:54–61. https://doi.org/10.1016/j.cbi.2015.11.020 PMID: 26626329

51. Laskowski M. [3] Trypsinogen and trypsin. Methods in enzymology. 1955; 2:26–36.

52. Asghari SM, Pazhang M, Ehtesham S, Karbalaei-Heidari HR, Taghdir M, Sadeghizadeh M, et al. Remarkable improvements of a neutral protease activity and stability share the same structural origins. Protein Engineering Design and Selection. 2010; 23(8):599–606.

53. Li H, Pu J, Wang Y, Liu C, Yu J, Li T, et al. Comparative study of the binding of Trypsin with bifendate and analogs by spectrofluorimetry. Spectrochimica Acta Part A: Molecular and Biomolecular Spectroscopy. 2013; 115:1–11.

54. Lakowicz JR, Weber G. Quenching of fluorescence by oxygen. Probe for structural fluctuations in macromolecules. Biochemistry. 1973; 12(21):4161–70. PMID: 4795686

55. Guan Y, Zhang H, Wang Y. New insight into the binding interaction of hydroxylated carbon nanotubes with bovine serum albumin. Spectrochimica Acta Part A: Molecular and Biomolecular Spectroscopy. 2014; 124:556–63.

56. Gull N, Sen P, Khan RH, Kabir ud D. Interaction of Bovine (BSA), Rabbit (RSA), and Porcine (PSA) Serum Albumins with Cationic Single-Chain/Gemini Surfactants: A Comparative Study. Langmuir. 2009; 25(19):11686–91. https://doi.org/10.1021/la901639h PMID: 19788221

57. Sekar G, Vijayakumar S, Thanigaivel S, Thomas J, Mukherjee A, Chandrasekaran N. Multiple spectroscopic studies on the interaction of BSA with pristine CNTs and their toxicity against Donax faba. Journal of Luminescence. 2016; 170:141–9.

58. Guan J, Liu G, Cai K, Gao C, Liu R. Probing the interactions between carboxylated multi-walled carbon nanotubes and copper–zinc superoxide dismutase at a molecular level. Luminescence. 2015; 30 (5):693–8. https://doi.org/10.1002/bio.2807 PMID: 25351393

59. Chi Z, Liu R, Zhang H. Noncovalent interaction of oxytetracycline with the enzyme trypsin. Biomacromolecules. 2010; 11(9):2454–9. https://doi.org/10.1021/bm100633h PMID: 20681619

60. Naveenraj S, Anandan S, Kathiravan A, Renganathan R, Ashokkumar M. The interaction of sonochemically synthesized gold nanoparticles with serum albumins. Journal of pharmaceutical and biomedical analysis. 2010; 53(3):804–10. https://doi.org/10.1016/j.jpba.2010.03.039 PMID: 20456895

61. Kelly SM, Jess TJ, Price NC. How to study proteins by circular dichroism. Biochimica et Biophysica Acta (BBA)-Proteins and Proteomics. 2005; 1751(2):119–39.

62. Greenfield NJ. Using circular dichroism spectra to estimate protein secondary structure. Nat Protocols. 2007; 1(6):2876–90. http://www.nature.com/nprot/journal/v1/n6/suppinfo/nprot.2006.202_S1.html.

63. Kelly SM, Price NC. The use of circular dichroism in the investigation of protein structure and function. Current protein and peptide science. 2000; 1(4):349–84. PMID: 12369905

64. Homaei AA, Sajedi RH, Sariri R, Seyfzadeh S, Stevanato R. Cysteine enhances activity and stability of immobilized papain. Amino acids. 2010; 38(3):937–42. https://doi.org/10.1007/s00726-009-0302-3 PMID: 19479190

65. Kabsch W, Sander C. Dictionary of protein secondary structure: pattern recognition of hydrogen-bonded and geometrical features. Biopolymers. 1983; 22(12):2577–637. https://doi.org/10.1002/bip.360221211 PMID: 6667333

66. Zhao X, Liu R, Chi Z, Teng Y, Qin P. New insights into the behavior of bovine serum albumin adsorbed onto carbon nanotubes: comprehensive spectroscopic studies. The journal of physical chemistry B. 2010; 114(16):5625–31. https://doi.org/10.1021/jp100903x PMID: 20373820

67. Cheng X-X, Lui Y, Zhou B, Xiao X-H, Liu Y. Probing the binding sites and the effect of berbamine on the structure of bovine serum albumin. Spectrochimica Acta Part A: Molecular and Biomolecular Spectroscopy. 2009; 72(5):922–8.

68. Heinig M, Frishman D. STRIDE: a web server for secondary structure assignment from known atomic coordinates of proteins. Nucleic acids research. 2004; 32(suppl_2):W500–W2.

69. Zhao X, Hao F, Lu D, Liu W, Zhou Q, Jiang G. Influence of the surface functional group density on the carbon-nanotube-induced α-chymotrypsin structure and activity alterations. ACS applied materials & interfaces. 2015; 7(33):18880–90.

70. El-Sayed R, Bhattacharya K, Gu Z, Yang Z, Weber JK, Li H, et al. Single-walled carbon nanotubes inhibit the cytochrome P450 enzyme, CYP3A4. Scientific reports. 2016; 6:21316. https://doi.org/10.1038/srep21316 PMID: 26899743

71. Zuo G, Kang Sg, Xiu P, Zhao Y, Zhou R. Interactions Between Proteins and Carbon-Based Nanoparticles: Exploring the Origin of Nanotoxicity at the Molecular Level. Small. 2013; 9(9-10):1546–56. https://doi.org/10.1002/smll.201201381 PMID: 23038664

72. Wu E, Coppens M-O, Garde S. Role of Arginine in Mediating Protein–Carbon Nanotube Interactions. Langmuir. 2015; 31(5):1683–92. https://doi.org/10.1021/la5043553 PMID: 25575129

73. Hirano A, Tanaka T, Kataura H, Kameda T. Arginine Side Chains as a Dispersant for Individual Single-Wall Carbon Nanotubes. Chemistry-A European Journal. 2014; 20(17):4922–30.

74. Zhao D, Zhou J. Electrostatics-mediated α-chymotrypsin inhibition by functionalized single-walled carbon nanotubes. Physical Chemistry Chemical Physics. 2017; 19(2):986–95. https://doi.org/10.1039/c6cp04962a PMID: 27781229

75. Gu Z, Yang Z, Wang L, Zhou H, Jimenez-Cruz CA, Zhou R. The role of basic residues in the adsorption of blood proteins onto the graphene surface. Scientific reports. 2015;5.

76. Quan-Tao D, Guang-Hong Z, Hai-Ping F. Interaction between a functionalized single-walled carbon nanotube and the YAP65WW protein domain: A molecular dynamics simulation study. Chinese Physics Letters. 2012; 29(6):068701.

77. Calvaresi M, Hoefinger S, Zerbetto F. Probing the Structure of Lysozyme–Carbon-Nanotube Hybrids with Molecular Dynamics. Chemistry-A European Journal. 2012; 18(14):4308–13.

78. Kagan VE, Konduru NV, Feng W, Allen BL, Conroy J, Volkov Y, et al. Carbon nanotubes degraded by neutrophil myeloperoxidase induce less pulmonary inflammation. Nature nanotechnology. 2010; 5(5):354. https://doi.org/10.1038/nnano.2010.44 PMID: 20364135